AD-A160 429 MAXIMUM BOUNDED ENTROPY: APPLICATION TO TOMOGRAPHIC RECONSTRUCTION(U) ARMY BALLISTIC RESEARCH LAB ABERDEEN PROVING GROUND MD B R FRIEDEN ET AL. APR 85 1/1

UNCLASSIFIED BRL-TR-2650 F/G 14/5 NL

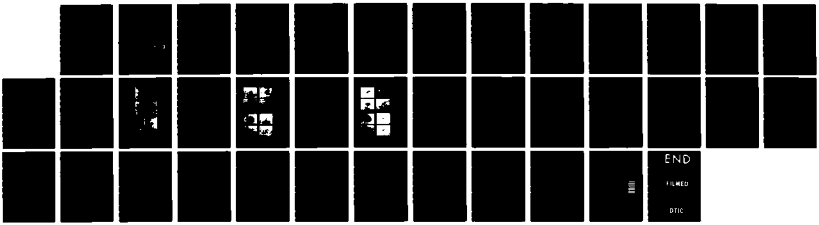

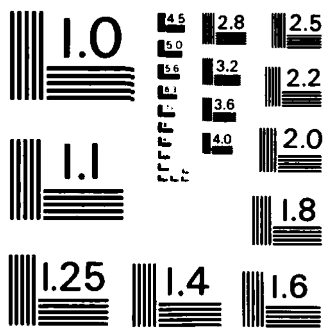

MICROCOPY RESOLUTION TEST CHART

NATIONAL BUREAU OF STANDARDS - 1963 - A

(12)

AD-A160 429

AD

US ARMY MATERIEL COMMAND

TECHNICAL REPORT BRL-TR-2650

MAXIMUM BOUNDED ENTROPY: APPLICATION TO TOMOGRAPHIC RECONSTRUCTION

B. Roy Frieden
Csaba K. Zoltani

April 1985

APPROVED FOR PUBLIC RELEASE; DISTRIBUTION UNLIMITED.

US ARMY BALLISTIC RESEARCH LABORATORY
ABERDEEN PROVING GROUND, MARYLAND

85 10 11 025

UNCLASSIFIED

SECURITY CLASSIFICATION OF THIS PAGE (When Data Entered)

REPORT DOCUMENTATION PAGE

READ INSTRUCTIONS BEFORE COMPLETING FORM

1. REPORT NUMBER: TECHNICAL REPORT BRL-TR-2650	2. GOVT ACCESSION NO.: AD-A160 429
3. RECIPIENT'S CATALOG NUMBER	
4. TITLE (and Subtitle): Maximum Bounded Entropy: Application to Tomographic Reconstruction	5. TYPE OF REPORT & PERIOD COVERED: Final
	6. PERFORMING ORG. REPORT NUMBER
7. AUTHOR(s): B. Roy Frieden* Csaba K. Zoltani	8. CONTRACT OR GRANT NUMBER(s)
9. PERFORMING ORGANIZATION NAME AND ADDRESS: US Army Ballistic Research Laboratory AMXBR-IBD Aberdeen Proving Ground, MD 21005-5066	10. PROGRAM ELEMENT, PROJECT, TASK AREA & WORK UNIT NUMBERS: 1L161102AH43
11. CONTROLLING OFFICE NAME AND ADDRESS: US Army Ballistic Research Laboratory ATTN: AMXBR-OD-ST Aberdeen Proving Ground, MD. 21005	12. REPORT DATE: April 85
	13. NUMBER OF PAGES: 38
14. MONITORING AGENCY NAME & ADDRESS (if different from Controlling Office)	15. SECURITY CLASS. (of this report): UNCLASSIFIED
	15a. DECLASSIFICATION DOWNGRADING SCHEDULE: NA

16. DISTRIBUTION STATEMENT (of this Report)

Approved for public release; distribution is unlimited.

17. DISTRIBUTION STATEMENT (of the abstract entered in Block 20, if different from Report)

18. SUPPLEMENTARY NOTES

*University of Arizona

19. KEY WORDS (Continue on reverse side if necessary and identify by block number)

Entropy	Tomography	Computerized Simulation
Alogrithms	Image Restoration	

gkl

20. ABSTRACT (Continue on reverse side if necessary and identify by block number)

We have investigated a new image restoring algorithm which utilizes maximum bounded entropy (MBE). It incorporates prior knowledge of both a lower and upper bound of the signal in the unknown object. Its outputs are maximum probable estimates of the object, under the following conditions: (a) the photons forming the image behave as classical particles; (b) the object is assumed to be biased toward a flat, gray scene in the absence of image data; (c) the object is modeled as consisting of high-gradient foreground details

20. Abstract (Cont'd):

riding on top of a smoothly varying background that must be estimated in a separate step; and (d) the image noise is Poisson. The proposed MBE estimator algorithm maximizes the sum of entropies of occupied and unoccupied photon sites. The result is an estimate of the object that is restricted to values inside the prescribed bounds. The algorithm was applied to the reconstruction of rod cross sections from tomographic viewing. In such a problem the object consists only of upper-and lower-bound values. We found that in the example only four projections were needed to provide a good reconstruction, and that 20 projections allowed the partial resolution of a single pixel-wide crack in one of the rods.

TABLE OF CONTENTS

FIGURE CAPTIONS

I. INTRODUCTION

It is widely appreciated that the faithfulness in estimation of an unknown object depends strongly upon what is known a priori about the object. In particular, the knowledge that the unknown object must be positive, called "positivity," has been well exploited in restoration schemes.[1-10] Calculational effort with reconstruction techniques is also

---

[1]A.C. Schell, "Enhancing the Angular Resolution of Incoherent Sources." Radio Electronic, Eng., Vol. 29, pp. 21-26, 1965.

[2]P.A. Jansson, R.H. Hunt, and E.K. Plyler, "Response Function for Spectral Resolution Enhancement," J. Opt. Soc. Am., Vol. 58, pp. 1665-1666, 1968.

[3]Y. Biraud, "A New Approach for Increasing the Resolving Power of Data Processing," Astron. Astrophys., Vol. 1, pp. 124-127, 1969.

[4]B.R. Frieden, "Restoring with Maximum Likelihood and Maximum Entropy," J. Opt. Soc. Am., Vol. 62, pp. 511-517, 1972.

[5]W.H. Richardson, "Bayesian Based Iterative Method of Image Restoration," J. Opt. Soc. Am., Vol. 62, pp. 55-59, 1972.

[6]L.B. Lucy, "An Iterative Technique for the Rectification of Observed Distributions," Astron. J., Vol. 79, pp. 745-754, 1974.

[7]S.J. Wernecke and L.R. D'Addario, "Maximum Entropy Image Reconstruction," IEEE Trans. Computers, Vol. C-26, pp. 351-364, 1977.

[8]S.F. Gull and G.J. Daniell, "Image Reconstruction from Incomplete and Noisy Data," Nature, Vol. 272, pp. 686-690, 1978.

[9]B.R. Frieden, "Image Restoration Using a Norm of Maximum Information," Proc. SPIE, Vol. 207, pp. 14-25, 1979.

[10]A.R. Davies, T. Cochrane, and O.M. Al-Faour, "The Numerical Inversion of Truncated Autocorrelation Functions," Optica Acta, Vol. 27, pp. 107-118, 1980.

considerably reduced when non-physical states are disallowed.[11-15] Positivity permits one to produce sharper edge gradients where the edge meets the known (or zero) background level[16] whereby the estimated gradient profile contains spatial frequencies that may appreciably exceed the cutoff frequency in the data.[3-4]

However, the high intensities near the top of the edge profile are not so enhanced. There, the data are far from the "forbidden" region of negative values; enforcing positivity upon already positive numbers does nothing to them. The question is, then, how can the gradient near the top of the edge profile be enhanced by enforcing some other prior knowledge?

Because a lower bound of zero works at low intensity values, it might be expected that knowledge of a finite upper bound b can produce the desired effect at the higher intensity values. In fact, this can be shown to be true, merely by reapplying the argument in Reference 16 to the upper-bound situation. The enhancement can be expected to be most effective if one has a least upper bound, and in particular, cases where the object attains it quite often across the scene. Ideally, it should attain the bound roughly as often as it attains zero or background values.

Objects of this kind arise diversely. In image restoration, the object might be a handwritten or printed page, where the white paper provides the upper bound and the print provides the lower bound. In spectroscopy, the object can be an absorption spectrum, which must lie between 0 and 100% levels.[17] In photography, advantage can be taken of the known fog and saturation density levels.[18] Or, in reconstruction tomography, the object

---

[11] R. Gordon, R. Bender, and G.T. Herman, "Algebraic Reconstruction Techniques (ART) for Three Dimensional Electron Microscopy and X-Ray Photography," J. Theor. Biol., Vol. 29, pp. 471-481, 1970.

[12] G. Minerbo, "MENT, A Maximum Entropy Algorithm for Reconstructing a Source from Projection Data," Comp. Graphics Image Processing, Vol. 10, pp. 48-68, 1979.

[13] A. Lent, "A Convergent Algorithm for Maximum Entropy Image Restoration with Medical X-Ray Applications," in SPSE Conference Proceedings, R. Shaw, ed., (SPSE, Washington, D.C., 1976), pp. 249-257.

[14] G.T. Herman, A. Lent, and S.W. Roland, "ART: Mathematics and Applications," J. Theor. Biol., Vol. 42, pp. 1-32, 1973.

[15] C.F. Barton, "Computerized Axial Tomography for Neutron Radiography of Nuclear Fuel," Trans. Amer. Nucl. Soc., Vol. 27, pp. 212-213, 1977.

[16] B.R. Frieden, "Estimation-A New Role for Maximum Entropy," in SPSE Conference Proceedings, R. Shaw, ed. (SPSE, Washington, D.C., 1976), pp. 261-265.

[17] P.A. Jansson, R.H. Hunt, and E.K. Plyler, "Resolution Enhancement of Spectra," J. Opt. Soc. Am., Vol. 60, pp. 596-599, 1970.

[18] B.R. Frieden, "Statistical Estimates of Bounded Optical Scenes by the Method of Prior Probabilities," IEEE Trans. Inform. Theory, Vol. IT-19, pp. 118-119, 1973.

might be machine parts or rods of known absorption coefficient immersed in a medium whose absorption coefficient is also known. If the rods are denser than the medium, they provide the upper bound in absorption, the medium providing the lower. We shall simulate this case in particular examples below.

In applications of this type one may have to choose the bounds depending on the purpose for forming the tomographic image. If the purpose is to visualize imperfections in the rods, it is important that the imperfections as well as the rods have absorption values that lie between the prescribed bounds (0,b). Otherwise the imperfections will not be augmented by enforcing the bounds. The simplest of imperfections--cracks--satisfy the bounds for the rods since where they occur a level b has merely been replaced by a 0. This case in particular will be considered below in the simulations. If, on the other hand, the imperfections are in the form of impurities with higher absorption embedded in the rods, e.g., an admixture of another substance that was inadvertently added during manufacture, then level b should be replaced by a proper b' exceeding b.

We follow the approach of Reference 4 and model the object as an array of photon counts m_n, n=1, ..., M=m, where m_n denotes the number of photons absorbed (in the tomographic case of interest) at position x_n in the object. Let Δo represent the energy increment represented by each count. Then an object o relates to its counts through

$$o = m\Delta o. \tag{1a}$$

We seek the most probable object o consistent with two known bounds

$$0 < o_n < b, \; n = 1, \cdots, M. \tag{1b}$$

II. IMAGE MODELING

A. Object Model

In this section we discuss a model of the object. Let the photons in question be x rays, as for example in tomography. These have low quantum degeneracy[19] and hence behave statistically like discrete or Boltzmann particles. This is one aspect of the model. Another aspect is the mean object ⟨o⟩. By the law of large numbers,[20] as the number of photons approaches infinity o will approach ⟨o⟩. Hence the numbers ⟨o⟩ act as "biases" for o. Since biasing is a profound effect, it must be closely

[19] R. Kikuchi and B.H. Soffer, "Maximum Entropy Image Restoration. I. The Entropy Expression," J. Opt. Soc. Am., Vol. 67, pp. 1656-1665, 1977.

[20] B.R. Frieden, Probability, Statistical Optics and Data Testing, Springer-Verlag, New York, 1983.

considered. If a form is assumed for $\langle o \rangle$, then o can only fluctuate probabilistically about it. How can we model $\langle o \rangle$?

An important aspect of the estimate o will be its reliability. Again, using the example of rods, if o shows a crack or pit, can it be trusted? The detail called "a crack" consists of a strong local departure from grayness that is, it has an abrupt decrease from b to 0 and corresponding large gradient. Hence, if we knew that o only shows small departures from grayness, we could trust the crack detail. On the other hand, we found that numbers $\langle o \rangle$ act as biases for o. It follows then that if numbers $\langle o \rangle$ were flat or constant

$$\langle o_n \rangle = \frac{b}{2} = \text{constant}, \qquad n = 1, \ldots, M, \tag{2}$$

and if we knew this to be true, then reliability could be so built into the estimated o.

The requirement (2) can be nearly true if the object consists of half background (with but a few rods), but it will not be rigorously true unless the object is only background (a most uninteresting case). However, the approximation has been used successfully to process astronomical pictures.[21]

Similarly, if the object field is packed with rods, requirement (2) will be far from satisfied. In this case an assumption of (2) will produce errors in the estimate; however, these will tend to be errors of "omission" only. That is, certain details will be missed, but no artifacts will tend to be created. Again, the reconstruction of a crack will be viewed as probably truthful. However, some cracks might be missed as the price paid. The false alarm rate will be low, but perhaps so will be the detection rate. Empirical tests may establish the rates in particular applications. (Note: empirically the theoretical possibility of a low detection rate was not borne out. See the Applications section below.) We shall adapt condition (2) as the second aspect of the object model.

B. A Priori Probability of an Object

Given the particle-like behavior of the photons, the knowledge of bounds (1b) and the assumption of a gray mean object (2), we are ready to form Pl(o), the a priori probability of a photon-count object o. This will be the probability that m indistinguishable particles are distributed in any order within M cells, where each cell can hold anywhere from 0 to $b/\Delta o$ particles. This obeys the binomial statistic

$$P_1(o) = \prod_{n=1}^{M} \frac{(b/\Delta o)!}{m_n!(b/\Delta o - m_n)!} \, p_n^{m_n} \, q_n^{b/\Delta o - m_n},$$

$$m_n = \frac{o_n}{\Delta o}, \qquad p_n = \frac{\langle o_n \rangle}{b}, \qquad q_n = 1 - p_n. \tag{3}$$

---

[21] B.R. Frieden and D.C. Wells, "Restoring with Maximum Entropy. III. Poisson Sources and Backgrounds," J. Opt. Soc. Am., Vol. 68, pp. 93-103, 1978.

In effect, the x rays are being treated like electrons, since this is also the likelihood expression for Fermi-Dirac particles. [Note: A more rigorous derivation of (3) from the standpoint of photon (not particle) statistics is given in Appendix A.] In particular for the mean object (2), this becomes

$$P_1(o) = (1/2)^{Mb/\Delta o} \prod_{n=1}^{M} \frac{(b/\Delta o)!}{m_n!(b/\Delta o - m_n)!}$$

$$= \text{const.} \times \prod_{n=1}^{M} \frac{1}{(o_n/\Delta o)!(b/\Delta o - o_n/\Delta o)!}, \tag{4}$$

the sought expression.

C. Image Model

The rest of the theory in this paper follows that of a previous paper.[21] The theory makes the following assumptions about the image data formed from the unknown object o:

(1) The image $i_1, \ldots, i_M = i$ suffers from noise $n_1, \ldots, n_M = n$ and rides atop a known background profile $B_1, \ldots, B_M \equiv B$ such that

$$i_m = \sum_{n=1}^{M} o_n s(x_m - x_n) + B_m + n_m. \tag{5}$$

The quantity s is the point spread function of the imagery. In computer tomography, it is the rayed function resembling the British Union Jack, with one ray for each projection.

Thus, there are now two sets of unknowns, o and n. Background B is assumed known by the use of some prefiltering operation upon the image, such as median windowing it.[22-24] (2) The noise n is Poisson. This is indeed the case when using modern imaging arrays in astronomy[21] and in computer tomography.[25]

---

[22] B.R. Frieden, "New Restoring Algorithm for the Preferential Enhancement of Edge Gradients," J. Opt. Soc. Am., Vol. 66, pp. 280-283, 1976.

[23] N.C. Gallagher and G.L. Wise, "Passband and Stopband Properties of Median Filters," Proceedings of the 1980 Conference on Information Sciences and Systems, Princeton University, New Jersey, 1980, pp. 303-307.

[24] B.R. Frieden, "Some Statistical Properties of the Median Window," Proc. SPIE, Vol. 373, pp. 219-224, 1981.

[25] H.H. Barrett and W. Swindell, Radiological Imaging, Academic Press, New York, 1981.

III. THE ALGORITHM

A. Net Likelihood Function

Taking a conventional probabilistic approach, we seek unknowns o and n that are jointly maximum probable,

$$P(o,n) = \text{maximum}, \tag{6}$$

subject to the data. From elementary considerations

$$P(o,n) = P_1(o)P_2(n|o). \tag{7}$$

We already know $P_1(o)$; see Equation 4.

The conditional probability $P_2(i|o)$ defines the fluctuations in i given one object o. The noise was assumed to be Poisson on the image with the image given as photon counts. If each count consists of an energy increment i, then the image intensity i corresponds to $i/\Delta i$ counts. Then, assuming independent image values, we have

$$P_2(i|o) = \prod_{m=1}^{M} \frac{a_m^{\,i_m/\Delta i} e^{-a_m}}{(i_m/\Delta i)!} \equiv P(n|o) \tag{8}$$

where a is the noiseless signal image count. By Equation (5),

$$a_m \equiv \frac{\langle i \rangle}{\Delta i} = \Delta i^{-1} \left(\sum_{n=1}^{M} o_n s(x_m - x_n) + B_m \right). \tag{9}$$

The final identity in (8) follows because with o fixed, by Equation (5) corresponding values of i_m and n_m have the same histogram. The net likelihood function is then, by identity (7), the product of Equations (4) and (8).

B. Restoring Principle

The principle of restoration is to maximize P(o,n) through choice of o and n subject to the image data i^{data} obeying (5). We shall also assume that the total energy E in the object is known, e.g., by conservation of energy from the image data. It is mathematically convenient to maximize ln P(o,n), instead of P(o,n) which gives the same solution. Also, we add the data and energy constraints to the objective function via Lagrange multipliers λ and μ . Accordingly, by Equations 6 and 7 we have to maximize the function

$$\ln P_1(o) + \ln P(n|o) - \sum_{m=1}^{M} \lambda_m (i_m - i_m^{data}) - \mu(\Sigma\, o_n - E) \tag{10}$$

through choice of n ,o and the Lagrange multipliers. Then by Equations (4) and (8) the objective function is

$$- \sum_n (o_n/\Delta o) \ln(o_n/\Delta o) - \sum_n (b/\Delta o - o_n/\Delta o) \ln(b/\Delta o - o_n/\Delta o)$$

$$+ \ln P(n|o) - \sum_m \lambda_m (i_m - i_m^{data}) - \mu(\Sigma\, o_n - E) = \text{maximum} . \tag{11}$$

The first sum is the Shannon entropy of the object, while the second is the Shannon entropy of the unfilled photon sites within each pixel. In other words, we have filled entropy plus unfilled entropy. This appears to be the natural way to accommodate an upper bound into a maximum entropy approach. (See also Reference 18.)

C. Net Restoring Algorithm

The solution to (11) is found[21] by substituting in the expression (11) Equation (8) for $P(n|o)$ and Equation (5) for i_m; and by the usual rules of calculus, equating to 0 in turn the partial derivatives of the objective function $\partial/\partial o_n$ (n fixed) and $\partial/\partial n_m$ (o fixed). Also, two approximations are made: a large enough number of photons are assumed present so that the Poisson law (8) may be approximately replaced by a normal law whose variance equals the mean; and the signal image a is assumed to be smooth and slowly varying. With these approximations the solution is an o obeying

$$i_m^{data} = [\, \sum_{n=1}^{M} o_n s(x_m - x_n) + B_m \,]\; e^{-1-\Lambda_m/\rho}, \quad m = 1,\ldots,M \tag{12a}$$

$$E = \sum_{n=1}^{M} o_n , \tag{12b}$$

$$o_n = \frac{b}{1 + \exp\left[\, \Gamma + \sum_m \Lambda_m s(x_m - x_n)\right]}, \quad n = 1, \ldots, M \tag{12c}$$

$$\Gamma \equiv \mu\Delta o, \qquad \Lambda_m \equiv \lambda_m \Delta o, \qquad \rho \equiv \Delta o/\Delta i. \tag{12d}$$

Thus, o represented through (12c) in terms of M + 1 free parameters Γ, Λ, must obey the M + 1 data Equations 12a,b. This is our maximum bounded entropy (MBE) restoring algorithm. We can see from the form of Equation 12c that the estimated o_n cannot have values outside the interval (0,b). The prescribed quantity ρ, defined at (12d), is called the "sharpness parameter." A higher value of ρ increases the resolution of the output o. Typically a value $\rho = 50$ causes a modest increase in resolution, while $\rho = 200$ causes a high increase. This behavior is consistent with its definition in (12d): If one inputs a high ρ , he is assuming that the object intrinsically consists of jumps Δo in intensity much exceeding those in the given image. This causes a "jumpier" and hence higher-resolved output. Other properties of ρ are discussed in Reference 21.

As mentioned before, B is the estimated background intensity function. Background is defined as a slowly varying component of the image data which intrinsically lacks resolution and hence is incapable of being restored further. The function B may be estimated by purposely blurring the input image, either by convolution with (say) a pillbox function[21] or by the use of a median window. The latter approach is recommended when the object details of interest have a known largest support. In this case, the use of a circular, filled ·ʼndow of diameter equal to twice (or more) this support value should be used. The output of this operation is "blind" to these object details, and hence only "sees" the background. Although this approach is more time-consuming than the convolution approach mentioned above, it gives a more accurate estimate of the background.

IV. APPLICATIONS TO COMPUTER TOMOGRAPHY

The preceding algorithm has been developed for any imaging situation where (a) the photons behave like particles, (b) the object is bounded by intensity levels 0 and b where b is a least upper bound to intensity, (c) the object consists of a slowly varying background function plus a foreground function whose details it is desired to restore, (d) the image is formed convolutionally from the object via a known point spread function, and (e) the image suffers from Poisson noise.

There are many cases where these conditions are satisfied in particular the case of computer tomographic imaging. Suppose that the "back-projected" image[25] is the given data i^{data}. This is known to connect with the absorptance object o via convolution with a Union Jack point spread function, for example such as in Figure 1a. Each arm of the pattern is formed by a projection in that direction. Hence in this example we are working with four projections.

The objects of interest are rods immersed in a medium. The rod cross sections comprise our foreground details. The absorptances of the rods are known to be at level b, i.e., all are at the upper bound; clearly, this is an ideal application of the approach. The absorptance of the medium is also known, but for consistency in the approach we estimate it (below). A typical object of this type is shown in Figure 1b, where the object rods are shown within a large cylinder. Everything beyond the cylinder is at 0 level. Intensity levels have been logarithmically stretched so as to enable the background to be seen: it is at 5% of the foreground. Hence the object has high contrast.

Notice that the foreground rod cross sections consist of three shapes approximating circles, the largest on top, smallest to the lower left. Each pixel is one detector-width wide, i.e., contains only one ray from a given projection. Hence, the back-projected image of this object will suffer severe spillover of energy from the broadest rod into the other two, and vice versa. In other words, there will be severe blur present. This was to provide an "acid-test" of the approach.

The spread function 1(a) was convolved in the computer with 1(b) to produce the back-projected image. This was made a Poisson noise process with a signal-to-noise ratio (S/N) of 10:1 at the brightest pixel in the image, Figure 1c. The image is quite noisy, since S/N falls off as the square root of intensity and hence is much less than 10:1 at most points in the scene. The principal blur is visually along the four projection directions, as would be expected. This image also suffers from numerous artifact "sources" due to the chance crossing of rays from different projections.

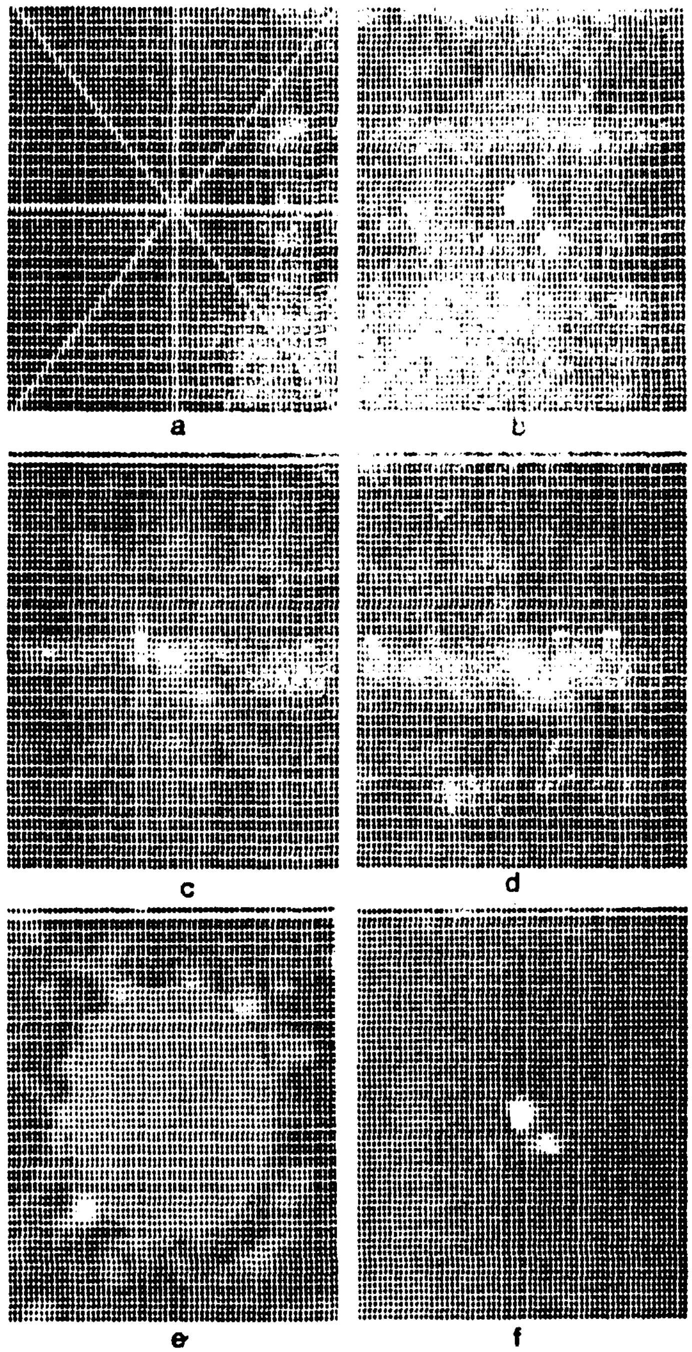

Figure 1a. Point Spread Function (Logarithm of Intensities).
b. Object (Logarithm of Intensities).
c. Poisson Image, S/N = 10.
d. Image Filtered Reconstruction Using $\rho = 200$.
e. Estimated Background B.
f. MBE Reconstruction Using $\rho = 200$.

To speed up the MBE algorithm (12a-d) we programmed it assuming a Gaussian point spread function s to be present. A Gaussian spread function is separable in the x and y directions. This permits the algorithm to be applied one dimensionally, first to the rows, then to the columns, of the image.[21] But the actual point spread function is not Gaussian, as is seen in Figure 1a. Hence, we had to filter the Poisson image into a Gaussian form, essentially dividing out the Union Jack and multiplying by the Gaussian. This output image is called the "prefiltered image." Using a standard deviation = 2 pixels in the Gaussian spread function, we obtained Figure 1d. Notice that the rayed appearance of the Poisson image 1(c) has been somewhat reduced. This is due to the Gaussian falloff of the new point spread function. However, some artifacts linger on. This image comprises i^{data}, the input to the MBE algorithm.

Since the image has been filtered, the background region has been changed from its value in the object. Hence, it has to be estimated. To do this, we took advantage of knowing that the rods are rather packed near the center, so that beyond a radius of about 16 pixels only background occurs (out to the cylinder walls). Hence, an average was taken over this region in 1(d) to infer the new background level. Background function B was then made to be this constant value out to the cylinder walls, and thereafter the image 1(d) itself; the latter because, beyond the walls there is known to be no foreground object. This background image is shown in Figure 1e. Numerous artifacts in the form of "blobs" can be seen outside the walls. These are due to imperfect prefiltering of the Union Jack into the Gaussian. However, they are in actuality much weaker than seen: we gray-scale stretched so as to render them visible. Also, since these lie outside the region of interest (the foreground object details), they do not much interfere with the MBE outputs.

Knowing i^{data} and B, we can now use the MBE routine. The use of a sharpness parameter 200 resulted in the restoration shown in Figure 1f. This is a pretty fair reconstruction of the original object 1(b). Its good aspects are (a) complete resolution of the three rods; compare with the resolution present in 1(c) or 1(d); (b) an almost absence of artifacts (one is visible on the lower left); (c) very strong edge-gradients at the rod boundaries; (d) true absorptance values within the restored rods (white corresponds to level b); and (e) faithful reconstruciton of the top rod's shape, most probably because it has the most energy of the three and hence suffered from noise propagation the least. The bad aspects are (a) faulty shape in the reconstructed, lower-right rod; and (b) strongly underestimating the intensity in the lower-left rod--it is almost not visible. But, considering that these results followed from the use of only four projection directions, we considered them encouraging.

We proceeded to try, in the same way, the case of 20 projections. Corresponding results are shown in Figure 2(a-e). In Figure 2e is shown the MBE output for $\rho = 200$. This is superior to the corresponding four-projections output in Figure 1f, as was expected. In particular, resolution is very high, shapes are more faithfully reconstructed, artifacts are still low, and even the weak, lower-left source is (now) strongly restored.

We also compared these results with results by the maximum entropy (ME) algorithm for the same data. Notice that in the objective function (11) if b

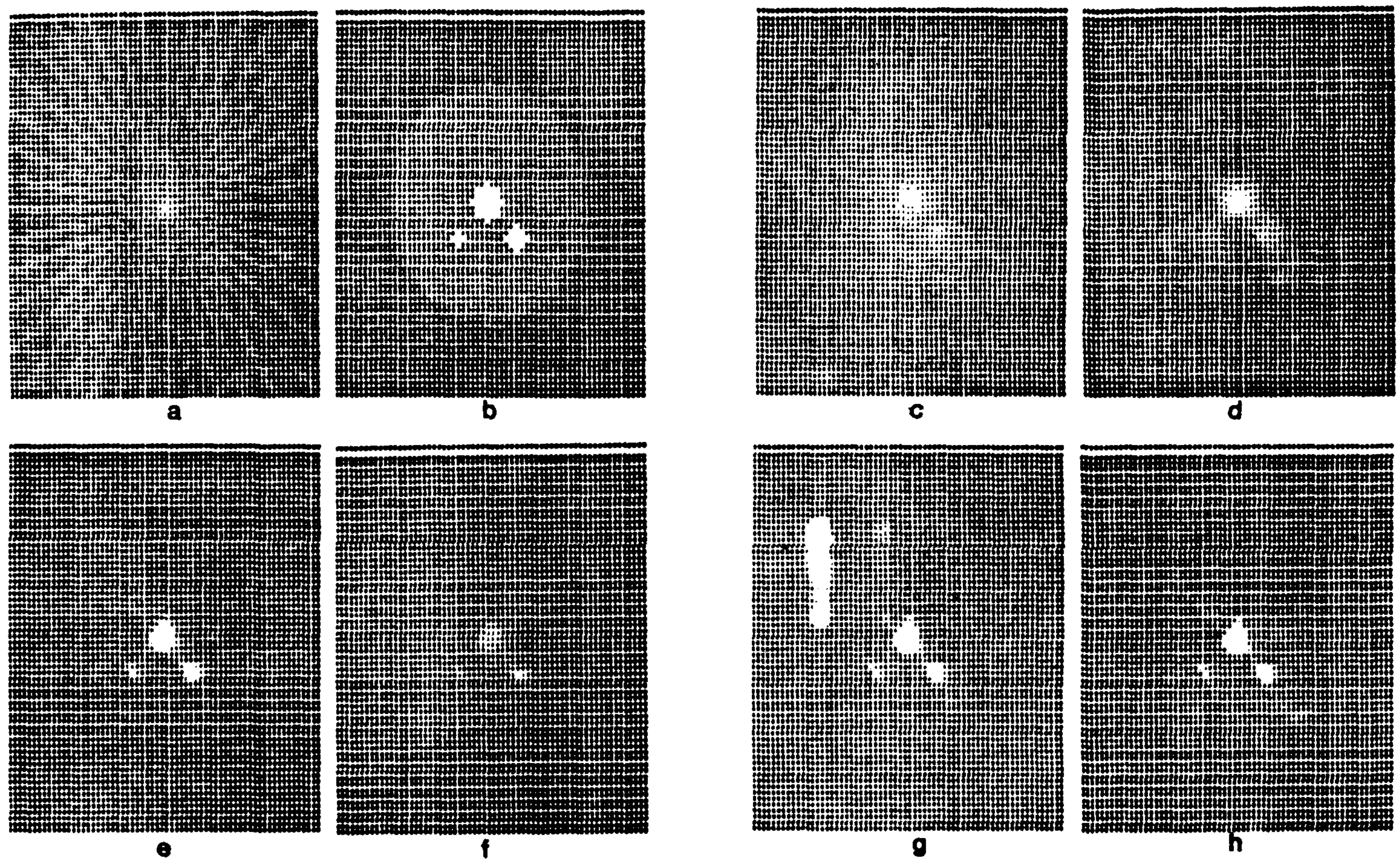

Figure 2a. Point Spread Function (Logarithm of Intensities).
b. Object (Logarithm of Intensities).
c. Poisson Image, SNR = 10.
d. Image Filtered into Gaussian Form, $\sigma = 2$.
e. MBE Reconstruction Using $\rho = 200$.
f. ME Reconstruction Using $\rho = 200$.
g. MBE Reconstruction Using $\rho = 300$.
h. MBE Reconstruction Using $\rho = 400$.

is made very large the second sum is effectively independent of choice o, i.e. it is a constant. Therefore, in this case the algorithm simply maximizes entropy, the first sum and the MBE algorithm becomes the ME algorithm. Hence, we made b twice the known upper bound (any further increase did not significantly change the output). The resulting ME restoration is shown in Figure 2f. This is a softer, lower-resolution estimate than before. The lower-left object is now barely detected. We conclude that the MBE algorithm with a good estimate of the upper bound b has a strong advantage over the maximum entropy (ME) algorithm.

In order to observe the effect of increased ρ upon the reconstruction, we now increased ρ to a value 300, with output in Figure 2g, and to a value 400, with output in Figure 2h (level b was once more at its true value). There is some increase in resolution, but it is apparent that this is saturating. The envisioned application to rod cross sections is to detect defects, particularly cracks, in the rods. As an example we included a one pixel wide crack in a rod. So narrow a crack furnishes an acid test for the algorithm. We again used 20 projections. Results are shown in Figure 3. The cracked rod is the top one, as shown in 3b. The overall object is otherwise the same as in Figure 2b. The Poisson image in 3(c) does show a gray, nebulous shape in the vicinity of the crack. However, this cannot be definitively used as an indicator for a crack, since image 2(c) also has a gray, nebulous shape there whereas its object did not have a crack. Evidently, some of the gray shape is due to the particular noise values chosen, which are about the same in both cases.

We prefiltered the Poisson image into its Gaussian form in Figure 3d, now using a σ of 1.5 (smaller than in Figure 2d). We then restored this by MBE in 3(e), using a ρ of 200. This again sharply restores the rod cross sections, but now with a notch in the top rod. This notch exactly corresponds in position to the crack. Comparison with the corresponding rod reconstruction in Figure 2e, where the object did not have a crack, shows a decisive difference. It is apparent that the crack has definitely been reconstructed in 3(e).

Figure 3f shows the result of now using MBE with $\rho = 400$. Higher resolution is attained, with the crack slightly better restored. This should be compared with reconstruction Figure 2h, where the crack did not exist in the object.

A better comparison with results in Figure 2 is obtained if the same σ as in Figure 2 were used in the prefiltering step in both cases. Accordingly, we filtered image 3(c) into a Gaussian form using, $\sigma = 2$. The result is Figure 3g. This image was fed into MBE using $\rho = 400$, with the result 3(h). Comparison with the corresponding uncracked restoration Figure 2h shows a definite restoration of the crack, although not quite as vividly as in 3(e) or 3(f). Evidently, the use of a smaller σ helped in this example.

We may summarize these results by stating that MBE can restore one pixel wide cracks in the rods with high reliability. This result is obtained for the high-contrast objects tested here, assuming 20 or more projections, and with S/N the order of 10:1 (or better). Thus, the biasing of the outputs toward a flat, gray scene did not cause the algorithm to miss crack details under these conditions. (See Object Model section.) We have not tested the

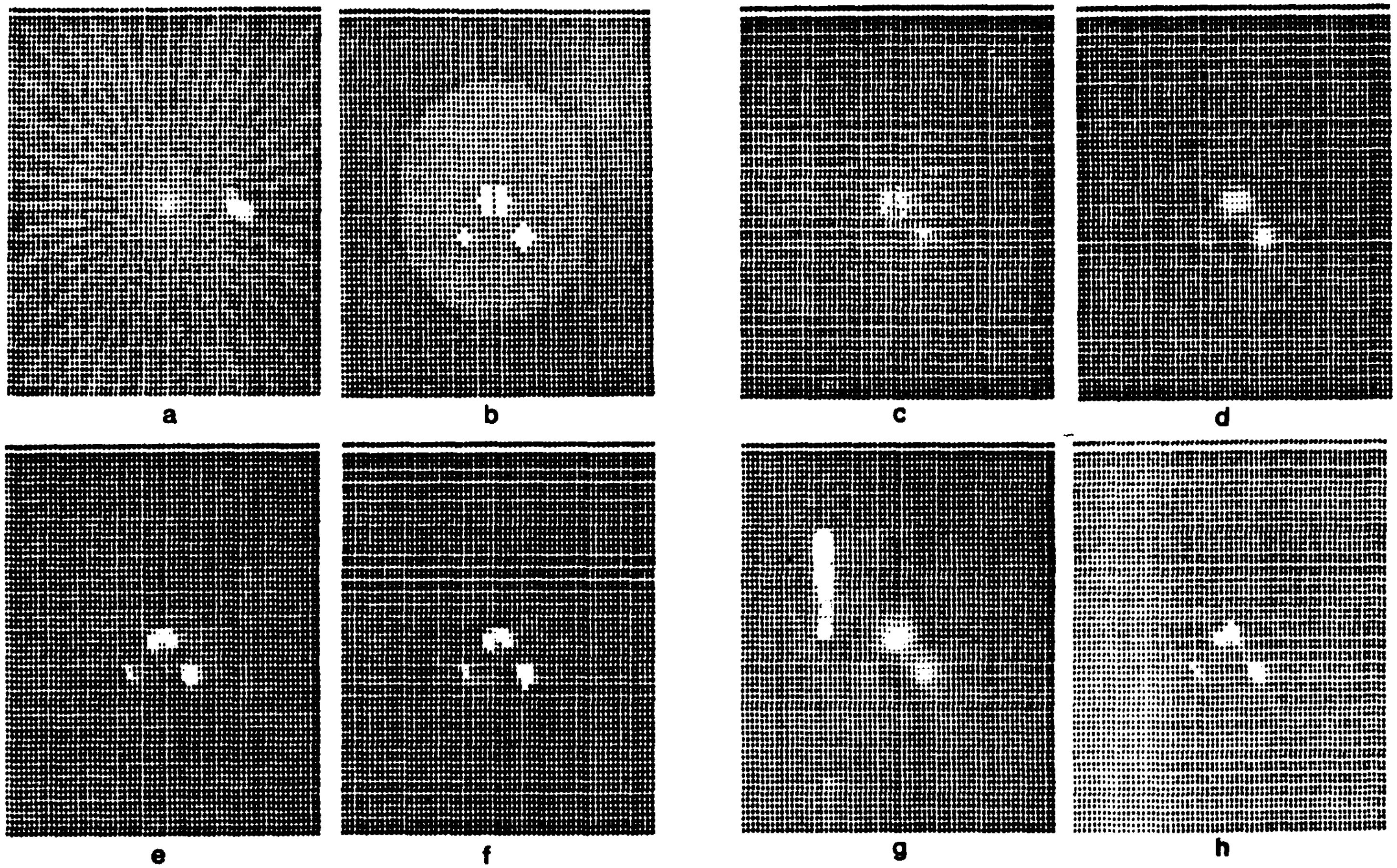

Figure 3a. Point Spread Function (Logarithm of Intensities).
b. Object (Logarithm of Intensities).
c. Poisson Image, SNR = 10.
d. Image Filtered into Gaussian Form, $\sigma = 1.5$.
e. MBE Reconstruction Using $\rho = 200$.
f. MBE Reconstruction Using $\rho = 400$.
g. Image (c) Filtered into Gaussian Form, $\sigma = 2$.
h. MBE Reconstruction Using $\rho = 400$.

algorithm on low-contrast objects or with lower S/N in the image. In the tested case, the crack was only partially restored, producing a distorted image of the rod. In practical applications it might not be recognized as a crack, since also the smaller undamaged rods were distorted. However, one can expect a good restoration of cracks wider than one pixel.

V. CONCLUSIONS

The knowledge of a least signal upper bound is very effective in enhancing the resolution of image reconstructions. The proviso is that this bound be met over a substantial part of the object field. The number of projections that are needed for high quality outputs by the suggested method can be quite small, ranging from 4 to 20, depending on accuracy requirements. In a sample problem rod cross sections could be accurately reconstructed with very high edge gradients, and one-pixel-wide cracks can be restored.

The time requirements for the 64 x 64 pixel cases shown were about 8 s of CPU time on a Cyber 135 mainframe computer. The time requirement is proportional to the area of the image to be processed expressed in pixels.

ACKNOWLEDGMENTS

This work was partially supported by funds provided by the Army Research Office. It was also supported by a visitor's stipend of the Netherlands Organization for Pure Research (Z.W.O.), while one of us (BRL) was on sabbatical leave at the University of Groningen, the Netherlands.

REFERENCES

1. A.C. Schell, "Enhancing the Angular Resolution of Incoherent Sources." Radio Electronic, Eng., Vol. 29, pp. 21-26, 1965.

2. P.A. Jansson, R.H. Hunt, and E.K. Plyler, "Response Function for Spectral Resolution Enhancement," J. Opt. Soc. Am., Vol. 58, pp. 1665-1666, 1968.

3. Y. Biraud, "A New Approach for Increasing the Resolving Power of Data Processing," Astron. Astrophys., Vol. 1, pp. 124-127, 1969.

4. B.R. Frieden, "Restoring with Maximum Likelihood and Maximum Entropy," J. Opt. Soc. Am., Vol. 62, pp. 511-517, 1972.

5. W.H. Richardson, "Bayesian Based Iterative Method of Image Restoration," J. Opt. Soc. Am., Vol. 62, pp. 55-59, 1972.

6. L.B. Lucy, "An Iterative Technique for the Rectification of Observed Distributions," Astron. J., Vol. 79, pp. 745-754, 1974.

7. S.J. Wernecke and L.R. D'Addario, "Maximum Entropy Image Reconstruction," IEEE Trans. Computers, Vol. C-26, pp. 351-364, 1977.

8. S.F. Gull and G.J. Daniell, "Image Reconstruction from Incomplete and Noisy Data," Nature, Vol. 272, pp. 686-690, 1978.

9. B.R. Frieden, "Image Restoration Using a Norm of Maximum Information," Proc. SPIE, Vol. 207, pp. 14-25, 1979.

10. A.R. Davies, T. Cochrane, and O.M. Al-Faour, "The Numerical Inversion of Truncated Autocorrelation Functions," Optica Acta, Vol. 27, pp. 107-118, 1980.

11. R. Gordon, R. Bender, and G.T. Herman, "Algebraic Reconstruction Techniques (ART) for Three Dimensional Electron Microscopy and X-Ray Photography," J. Theor. Biol., Vol. 29, pp. 471-481, 1970.

12. G. Minerbo, "MENT, A Maximum Entropy Algorithm for Reconstructing a Source from Projection Data," Comp. Graphics Image Processing, Vol. 10, pp. 48-68, 1979.

13. A. Lent, "A Convergent Algorithm for Maximum Entropy Image Restoration with Medical X-Ray Applications," in SPSE Conference Proceedings, R. Shaw, ed., (SPSE, Washington, D.C., 1976), pp. 249-257.

14. G.T. Herman, A. Lent, and S.W. Roland, "ART: Mathematics and Applications," J. Theor. Biol., Vol. 42, pp. 1-32, 1973.

15. C.F. Barton, "Computerized Axial Tomography for Neutron Radiography of Nuclear Fuel," Trans. Amer. Nucl. Soc., Vol. 27, pp. 212-213, 1977.

16. B.R. Frieden, "Estimation-A New Role for Maximum Entropy," in SPSE Conference Proceedings, R. Shaw, ed. (SPSE, Washington, D.C., 1976), pp. 261-265.

17. P.A. Jansson, R.H. Hunt, and E.K. Plyler, "Resolution Enhancement of Spectra," J. Opt. Soc. Am., Vol. 60, pp. 596-599, 1970.

18. B.R. Frieden, "Statistical Estimates of Bounded Optical Scenes by the Method of Prior Probabilities," IEEE Trans. Inform. Theory, Vol. IT-19, pp. 118-119, 1973.

19. R. Kikuchi and B.H. Soffer, "Maximum Entropy Image Restoration. I. The Entropy Expression," J. Opt. Soc. Am., Vol. 67, pp. 1656-1665, 1977.

20. B.R. Frieden, Probability, Statistical Optics and Data Testing, Springer-Verlag, New York, 1983.

21. B.R. Frieden and D.C. Wells, "Restoring with Maximum Entropy. III. Poisson Sources and Backgrounds," J. Opt. Soc. Am., Vol. 68, pp. 93-103, 1978.

22. B.R. Frieden, "New Restoring Algorithm for the Preferential Enhancement of Edge Gradients," J. Opt. Soc. Am., Vol. 66, pp. 280-283, 1976.

23. N.C. Gallagher and G.L. Wise, "Passband and Stopband Properties of Median Filters," Proceedings of the 1980 Conference on Information Sciences and Systems, Princeton University, New Jersey, 1980. pp. 303-307.

24. B.R. Frieden, "Some Statistical Properties of the Median Window," Proc. SPIE, Vol. 373, pp. 219-224, 1981.

25. H.H. Barrett and W. Swindell, Radiological Imaging, Academic Press, New York, 1981.

APPENDIX A

USE OF BOSE-EINSTEIN STATISTICS

APPENDIX A: USE OF BOSE-EINSTEIN STATISTICS

A more fundamental derivation of the a priori object law (3) follows by separately considering photon absorptions and transmissions through the object.*

Let E_n known photons be incident upon pixel n. This quantity is ordinarily known in computer tomography, since the incident energy upon the object is accurately monitored, and pixels toward the emergent side of the object are not strongly blocked by pixels on the incident side (most of the light passes unabsorbed through the object).

Next, consider the identity

$$E_n = m + (b/o - m) + (E_n - b/\Delta o). \tag{A1}$$

This describes the fate of the E_n photons as independently m absorptions, (b/o - m) transmissions and (E_n - b/o) transmissions. Let these three states have z, z', and z" degrees of freedom, respectively. Then the probability law for the E_n photons is

$$P(E_n) = P_z(m)P_z'(b/\Delta o - m)P_z"(E_n - b/\Delta o), \tag{A2}$$

where $P_z(k)$ is proportional to the Bose-Einstein statistics,[19]

$$P_z(k) = ((k + z - 1)!)/(k!(z - 1)!)\ p^k. \tag{A3}$$

By inspection, in the classical particle limit z large, this law goes over into a statistic

$$P_z(k) = p^k/k!\ . \tag{A4}$$

The probability law $P_z"$ in (A2) is merely a multiplicative constant independent of m and here may be ignored. Hence, in the classical particle limit z, z' large appropriate for x rays, Equation (A2) becomes proportional to a binomial statistic,

$$P(E_n)\ \alpha\ p_n{}^m/m!\ [q_n b/o-m/(b/\Delta o - m)]!\ . \tag{A5}$$

As the pixels n act independently, the net probability $P(E_1,\ldots,E_m)$ for all photons goes over into a product of factors (A5). This is of the form Equation 3, as was to be proved.

---

*We thank B.H. Soffer of Hughes Research Laboratories for the basic idea behind this proof.

DISTRIBUTION LIST

No. Of Copies	Organization
12	Administrator Defense Technical Info Center ATTN: DTIC-DDA Cameron Station Alexandria, VA 22304-6145
1	HQ DA DAMA-ART-M Washington, DC 20310
1	Commander US Army Materiel Command ATTN: AMCDRA-ST 5001 Eisenhower Avenue Alexandria, VA 22333-0001
1	Commander Armament R&D Center USA AMCCOM ATTN: SMCAR-TDC Dover, NJ 07801
1	Commander Armament R&D Center USA AMCCOM ATTN: SMCAR-TSS Dover, NJ 07801
1	Commander US Army Armament, Munitions and Chemical Command ATTN: SMCAR-ESP-L Rock Island, IL 61299
1	Director Benet Weapons Laboratory Armament R&D Center USA AMCCOM ATTN: SMCAR-LCB-TL Watervliet, NY 12189
1	Commander USA Aviation Research and Development Command ATTN: AMSAV-E 4300 Goodfellow Blvd. St. Louis, MO 63120
1	Director USA Air Mobility Research and Development Laboratory Ames Research Center Moffett Field, CA 94035
6	Commander US Army Research Office Durham ATTN: R. Ghirardelli D. Mann R. Singleton R. Shaw S. Chandra F. Oertel Research Triangle Park, NC 27709-2211
1	Commander USA Communications - Electronics Command ATTN: AMSEL-ED Fort Monmouth, NJ 07703
1	Commander USA Electronics Research and Development Command Technical Support Activity ATTN: DELSD-L Fort Monmouth, NJ 07703-5301
2	Commander USA AMCCOM ATTN: SMCAR-LCA-G, D.S. Downs J.A. Lannon Dover, NJ 07801
1	Commander USA AMCCOM ATTN: SMCAR-LC-G, S. Harris Dover, NJ 07801
1	Commander USA AMCCOM ATTN: SMCAR-SCA-T, L. Stiefel Dover, NJ 07801

DISTRIBUTION LIST

No. Of Copies	Organization
1	Commander USA Missile Command ATTN: AMSMI-R Redstone Arsenal, AL 35898
1	Commander USA Missile Command ATTN: AMSMI-YDL Redstone Arsenal, AL 35898
2	Commander USA Missile Command ATTN: AMSMI-RK, D.J. Ifshin W. Wharton Redstone Arsenal, AL 35898
1	Commander USA Tank Automotive Command ATTN: AMSTA-TSL Warren, MI 48090
1	Director USA TRADOC Systems Analysis Activity ATTN: ATAA-SL White Sands Missile Range, NM 88002
1	Commandant US Army Infantry School ATTN: ATSH-CD-CSO-OR Fort Benning, GA 31905
1	Commander US Army Development and Employment Agency ATTN: MODE-TED-SAB Fort Lewis, WA 98433
1	Office of Naval Research Department of the Navy ATTN: R.S. Miller, Code 432 800 N. Quincy Street Arlington, VA 22217
1	Navy Strategic Systems Project Office ATTN: R.D. Kinert, SP 2731 Washington, DC 20376

No. Of Copies	Organization
1	Commander Naval Air Systems Command ATTN: J. Ramnarace, AIR-54111C Washington, DC 20360
2	Commander Naval Ordnance Station ATTN: C. Irish P.L. Stang, Code 515 Indian Head, MD 20640
1	Commander Naval Surface Weapons Center ATTN: J.L. East, Jr., G-23 Dahlgren, VA 22448
2	Commander Naval Surface Weapons Center ATTN: R. Bernecker, R-13 G.B. Wilmot, R-16 Silver Spring, MD 20910
1	Commander Naval Weapons Center ATTN: R.L. Derr, Code 389 China Lake, CA 93555
2	Commander Naval Weapons Center ATTN: Code 3891, T. Boggs K.J. Graham China Lake, CA 93555
5	Commander Naval Research Laboratory ATTN: L. Harvey J. McDonald E. Oran J. Shnur R.J. Doyle, Code 6110 Washington, DC 20375
1	Commanding Officer Naval Underwater Systems Center Weapons Dept. ATTN: R.S. Lazar/Code 36301 Newport, RI 02840

DISTRIBUTION LIST

No. Of Copies	Organization
1	Superintendent Naval Postgraduate School Dept. of Aeronautics ATTN: D.W. Netzer Monterey, CA 93940
6	AFRPL (DRSC) ATTN: R. Geisler D. George B. Goshgarian J. Levine W. Roe D. Weaver Edwards AFB, CA 93523-5000
1	Air Force Armament Laboratory ATTN: AFATL/DLODL Eglin AFB, FL 32542-5000
2	AFOSR ATTN: L.H. Caveny J.M. Tishkoff Bolling Air Force Base Washington, DC 20332
1	AFWL/SUL Kirtland AFB, NM 87117
1	NASA Langley Research Center ATTN: G.B. Northam/MS 168 Hampton, VA 23365
6	National Bureau of Standards ATTN: J. Hastie M. Jacox T. Kashiwagi H. Semerjian S. Ray A.Carasso US Department of Commerce Washington, DC 20234
1	Applied Combustion Technology, Inc. ATTN: A.M. Varney P.O. Box 17885 Orlando, FL 32860
1	Atlantic Research Corp. ATTN: M.K. King 5390 Cherokee Avenue Alexandria, VA 22314
1	Atlantic Research Corp. ATTN: R.H.W. Waesche 7511 Wellington Road Gainesville, VA 22065
1	AVCO Everett Rsch. Lab. ATTN: D. Stickler 2385 Revere Beach Parkway Everett, MA 02149
1	Battelle Memorial Institute Tactical Technology Center ATTN: J. Huggins 505 King Avenue Columbus, OH 43201
2	Exxon Research & Eng. Co. ATTN: A. Dean M. Chou P.O. Box 8 Linden, NJ 07036
1	Ford Aerospace and Communications Corp. DIVAD Division Div. Hq., Irvine ATTN: D. Williams Main Street & Ford Road Newport Beach, CA 92663

DISTRIBUTION LIST

No. Of Copies	Organization
1	General Electric Company 235 Jade Lane Schenectady, NY 12309
1	Rockwell International Corp. Rocketdyne Division ATTN: J. E. Flanagan/HB02 6633 Canoga Avenue Canoga Park, CA 91304
1	General Motors Corporation Physics Department ATTN: R. Teets Warren, MI 48090
1	Hercules Powder Company Allegany Ballistics Lab. ATTN: R.R. Miller P.O. Box 210 Cumberland, MD 21501
1	Hercules, Inc. Bacchus Works ATTN: K.P. McCarty P.O. Box 98 Magna, UT 84044
1	Hercules, Inc. AFATL/DLDL ATTN: R.L. Simmons Eglin AFB, FL 32542
1	Honeywell, Inc. Defense Systems Division ATTN: D.E. Broden/ MS MN50-2000 600 2nd Street NE Hopkins, MN 55343
1	IBM Corporation ATTN: A.C. Tam Research Division 5600 Cottle Road San Jose, CA 95193

No. Of Copies	Organization
1	Director Lawrence Livermore National Laboratory ATTN: C. Westbrook Livermore, CA 94550
1	Lockheed Missiles & Space Co. ATTN: George Lo 3251 Hanover Street Dept. 52-35/B204/2 Palo Alto, CA 94304
3	Los Alamos National Lab ATTN: B. Nichols T7, MS-B284 C. Mader K. Hanson P.O. Box 1663 Los Alamos, NM 87544
1	Olin Corporation Smokeless Powder Operations ATTN: R.L. Cook P.O. Box 222 St. Marks, FL 32355
1	Paul Gough Associates, Inc. ATTN: P.S. Gough 1048 South Street Portsmouth, NH 03801
2	Princeton Combustion Research Laboratories, Inc. ATTN: M. Summerfield N.A. Messina 475 US Highway One Monmouth Junction, NJ 08852
1	Hughes Aircraft Company ATTN: T.E. Ward 8433 Fallbrook Avenue Canoga Park, CA 91303

DISTRIBUTION LIST

No. Of Copies	Organization
3	Sandia National Laboratories Combustion Sciences Dept. ATTN: R. Cattolica D. Stephenson P. Mattern Livermore, CA 94550
1	Sandia National Laboratories ATTN: M. Smooke Division 8353 Livermore, CA 94550
1	Science Applications, Inc. ATTN: R.B. Edelman 23146 Cumorah Crest Woodland Hills, CA 91364
1	Science Applications, Inc. ATTN: H.S. Pergament 1100 State Road, Bldg. N Princeton, NJ 08540
1	Aerojet Solid Propulsion Co. ATTN: P. Micheli Sacramento, CA 95813
3	SRI International ATTN: G. Smith D. Crosley D. Golden 333 Ravenswood Avenue Menlo Park, CA 94025
1	Stevens Institute of Tech. Davidson Laboratory ATTN: R. McAlevy, III Hoboken, NJ 07030
1	Teledyne McCormack-Selph ATTN: C. Leveritt 3601 Union Road Hollister, CA 95023
1	Thiokol Corporation Elkton Division ATTN: W.N. Brundige P.O. Box 241 Elkton, MD 21921

No. Of Copies	Organization
1	Thiokol Corporation Huntsville Division ATTN: D.A. Flanagan Huntsville, AL 35807
1	Thiokol Corporation Wasatch Division P.O. Box 524 Brigham City, UT 84302
1	United Technologies ATTN: A.C. Eckbreth East Hartford, CT 06108
2	United Technologies Corp. ATTN: R.S. Brown R.O. McLaren P.O. Box 358 Sunnyvale, CA 94086
1	Universal Propulsion Company ATTN: H.J. McSpadden Black Canyon Stage 1 Box 1140 Phoenix, AZ 85029
1	Veritay Technology, Inc. ATTN: E.B. Fisher P.O. Box 22 Bowmansville, NY 14026
1	Brigham Young University Dept. of Chemical Engineering ATTN: M.W. Beckstead Provo, UT 84601
1	California Institute of Tech. Jet Propulsion Laboratory ATTN: MS 125/159 4800 Oak Grove Drive Pasadena, CA 91109
1	California Institute of Technology ATTN: F.E.C. Culick/ MC 301-46 204 Karman Lab. Pasadena, CA 91125

DISTRIBUTION LIST

No. Of Copies	Organization
1	University of California, Berkeley Mechanical Engineering Dept. ATTN: J. Daily Berkeley, CA 94720
1	University of California Los Alamos Scientific Lab. ATTN: T.D. Butler P.O. Box 1663, Mail Stop B216 Los Alamos, NM 87545
2	University of California, Santa Barbara Quantum Institute ATTN: K. Schofield M. Steinberg Santa Barbara, CA 93106
1	University of Southern California Dept. of Chemistry ATTN: S. Benson Los Angeles, CA 90007
1	Case Western Reserve Univ. Div. of Aerospace Sciences ATTN: J. Tien Cleveland, OH 44135
1	Cornell University Department of Chemistry ATTN: E. Grant Baker Laboratory Ithaca, NY 14853
1	Univ. of Dayton Rsch Inst. ATTN: D. Campbell AFRPL/PAP Stop 24 Edwards AFB, CA 93523
1	University of Florida Dept. of Chemistry ATTN: J. Winefordner Gainesville, FL 32611
3	Georgia Institute of Technology School of Aerospace Engineering ATTN: E. Price W.C. Strahle B.T. Zinn Atlanta, GA 30332
2	University of Illinois Dept. of Mech. Eng. ATTN: H. Krier S.L. Soo 1206 W. Green St. Urbana, IL 61801
1	Johns Hopkins University/APL Chemical Propulsion Information Agency ATTN: T.W. Christian Johns Hopkins Road Laurel, MD 20707
1	University of Minnesota Dept. of Mechanical Engineering ATTN: E. Fletcher Minneapolis, MN 55455
4	Pennsylvania State University Applied Research Laboratory ATTN: G.M. Faeth K.K. Kuo H. Palmer M. Micci University Park, PA 16802
1	Polytechnic Institute of NY ATTN: S. Lederman Route 110 Farmingdale, NY 11735
1	Naval Coastal Systems Center Code 2210-C ATTN: J. Mittleman Panama City, FL 32407

DISTRIBUTION LIST

No. Of Copies	Organization
2	Cdr, AMCCOM ATTN: AMSMC-QAS-A J. Moskowitz J.M. Argento Dover, NJ 07801
1	Naval Ordnance Station Code 3023A Indian Head, MD 20640
1	Commander US Army White Sands Missile Range ATTN: STEWS-HP-T White Sands Missile Range, NM 88002
1	Naval Ordnance Station Code 5251 F ATTN: Dr. C. Dale Indian Head, MD 20640
1	University of California, San Diego Energy Center and Dep. Applied Mechanics ATTN: S.S. Penner La Jolla, CA 92037
1	SAI ATTN: N. Banks 626 Town Ct. Dr. Joppa, MD 21085
2	University of California Lawrence Livermore National Laboratory ATTN: Library A.C. Buckingham Livermore, CA 94550
1	University of Arizona Optical Sciences Center ATTN: B. Roy Frieden Tucson, AZ 85721
1	Oregon State College Department of Mathematics ATTN: Kennon Smith Corvallis, OR 97330
1	University of Michigan Department of Mechanical Engineering ATTN: C.M. Vest Ann Arbor, MI 48104
1	Southwest Research Institute Instrumentation Research Division 6220 Culebra Rd. San Antonio, TX 78228
1	Argonne National Laboratory Materials Science and Technology Division ATTN: W.A. Ellingson Argonne, IL 60439
1	Washington University Mallinckrodt Institute of Radiology ATTN: M.W. Vannier 510 S. Kingshighway St. Louis, MO 63110
2	Boeing Company Physics Technology Department ATTN: K.D. Friddell A.R. Lowrey Box 3999, M.S. 8C-23 Seattle, WA 98124
2	The Harshaw Chemical Company Crystal and Electronic Products Department ATTN: M.R. Farukhi C. Rozsa Solon, OH 44139
2	Hewlett-Packard Corp. ATTN: F. Charbonnier L. Bailey 1700 South Baker Street McMinnville, OR 97128

DISTRIBUTION LIST

No. Of Copies	Organization
1	Industrial Quality, Inc. ATTN: H. Berger P.O. Box 2397 Gaithersburg, MD 20879
1	MCI Optonix, Inc. ATTN: G. Zweig Horsehill Road P.O. Box 1 Cedar Knolls, NJ 07927
1	Princeton Scientific Instruments, Inc. ATTN: J.L. Lowrance P.O. Box 252 Kingston, NJ 08528
1	Scientific Research Associates, Inc. ATTN: H. McDonald P.O. Box 498 Glastonbury, CT 06033
1	Thorn EMI Gencom, Inc. ATTN: L.M. Lieberman 80 Express Street Plainview, NY 11803
3	Mayo Clinic Biodynamics Research Unit ATTN: E.L. Ritman J.H. Kinsey R.A. Robb 200 First Street, S.W. Rochester, MN 55901
1	University of California Donner Laboratory ATTN: T.F. Budinger Berkeley, CA 94720
1	George Washington University School of Engineering and Applied Science ATTN: R. Goulard Washington, DC 20052
1	Massachusetts Institute of Technology Laboratory for Information and Decision Systems ATTN: A.S. Willsky Cambridge, MA 02139
1	University of North Carolina Bio-Medical Engineering Department ATTN: F.A. DiBianca Chapel Hill, NC 27514
1	Hospital of the University of Pennsylvania Department of Radiology ATTN: G.T. Herman 3400 Spruce Street Philadelphia, PA 19104
1	University of Pittsburgh ATTN: D. Sashin Pittsburgh, PA 15213
1	Stanford University Department of Physics ATTN: A. Macovski Palo Alto, CA 94305
1	University of Utah Department of Mathematics ATTN: F. Stenger Salt Lake City, UT 84112
1	Dr. G. Morgan 1912 Sheffield Court Severn, MD 21144
2	Mathematics Research Center ATTN: B. Noble J. Nohel 610 Walnut Street Madison, WI 53706
1	Advanced Research and Applications Corporation ATTN: A.G. Lason 8150 Leesburg Pike Vienna, VA 22180

DISTRIBUTION LIST

No. Of Copies	Organization
1	General Electric Armament & Electrical Systems ATTN: M. J. Bulman Lakeside Avenue Burlington, VT 05401
2	Bell Laboratories ATTN: M. Sondhi F. Shepp Murray Hill, NJ 07971
1	BDM Corp. ATTN: T.P. Goddard 2600 Cearden Road North Bldg Monterey, CA 93940
1	General Electric Computer Research Medical Diagnostics Systems Program ATTN: T. Kincaid Schenectady, NY 12345
1	Shell Development Oil Co. ATTN: Dr. H. Vinegar P.O. Box 481 Houston, TX 77001
2	Princeton University Forrestal Campus Library ATTN: K. Brezinsky I. Glassman P.O. Box 710 Princeton, NJ 08540
1	Princeton University MAE Dept. ATTN: F.A. Williams Princeton, NJ 08544
2	Purdue University School of Aeronautics and Astronautics ATTN: R. Glick J.R. Osborn Grissom Hall West Lafayette, IN 47906
2	Purdue University School of Mechanical Engineering ATTN: N.M. Laurendeau S.N.B. Murthy TSPC Chaffee Hall West Lafayette, IN 47906
1	Rensselaer Polytechnic Inst. Dept. of Chemical Engineering ATTN: A. Fontijn Troy, NY 12181
2	Southwest Research Institute ATTN: R.E. White A.B. Wenzel 8500 Culebra Road San Antonio, TX 78228
1	Stanford University Dept. of Mechanical Engineering ATTN: R. Hanson Stanford, CA 94305
1	University of Texas Dept. of Chemistry ATTN: W. Gardiner Austin, TX 78712
1	University of Utah Dept. of Chemical Engineering ATTN: G. Flandro Salt Lake City, UT 84112
2	Virginia Polytechnic Institute and State University ATTN: J.A. Schetz R.T. Smith Blacksburg, VA 24061

DISTRIBUTION LIST

No. Of Copies	Organization

Aberdeen Proving Ground

Dir, USAMSAA
  ATTN: AMXSY-D
        AMXSY-MP, H. Cohen
Cdr, USATECOM
  ATTN: AMSTE-TO-F
Cdr, CRDC, AMCCOM
  ATTN: SMCCR-RSP-A
        SMCCR-MU
        SMCCR-SPS-IL

USER EVALUATION SHEET/CHANGE OF ADDRESS

This Laboratory undertakes a continuing effort to improve the quality of the reports it publishes. Your comments/answers to the items/questions below will aid us in our efforts.

1. BRL Report Number__________________________Date of Report____________

2. Date Report Received____

3. Does this report satisfy a need? (Comment on purpose, related project, or other area of interest for which the report will be used.)__________________

4. How specifically, is the report being used? (Information source, design data, procedure, source of ideas, etc.)____________________________________

5. Has the information in this report led to any quantitative savings as far as man-hours or dollars saved, operating costs avoided or efficiencies achieved, etc? If so, please elaborate.____

6. General Comments. What do you think should be changed to improve future reports? (Indicate changes to organization, technical content, format, etc.)

CURRENT ADDRESS

Name

Organization

Address

City, State, Zip

7. If indicating a Change of Address or Address Correction, please provide the New or Correct Address in Block 6 above and the Old or Incorrect address below.

OLD ADDRESS

Name

Organization

Address

City, State, Zip

(Remove this sheet along the perforation, fold as indicated, staple or tape closed, and mail.)

FOLD HERE

Director
US Army Ballistic Research Laboratory
ATTN: AMXBR-OD-ST
Aberdeen Proving Ground, MD 21005-5066

NO POSTAGE
NECESSARY
IF MAILED
IN THE
UNITED STATES

OFFICIAL BUSINESS

PENALTY FOR PRIVATE USE, $300

BUSINESS REPLY MAIL

FIRST CLASS PERMIT NO 12062 WASHINGTON, DC

POSTAGE WILL BE PAID BY DEPARTMENT OF THE ARMY

Director
US Army Ballistic Research Laboratory
ATTN: AMXBR-OD-ST
Aberdeen Proving Ground, MD 21005-9989

FOLD HERE

END

FILMED

12-85

DTIC